2009

A Frequency Agile, Distributed Sensor System to Address Space Weather Effects Upon Ionospherically Dependent Systems

D. D. Rice

J. V. Eccles

Jan Josef Sojka
Utah State University

J. W. Raitt

J. Brady

R. D. Hunsucker

Recommended Citation
Rice, D. D., J. V. Eccles, J. J. Sojka, J. W. Raitt, J. Brady, and R. D. Hunsucker (2009), A Frequency-Agile Distributed Sensor System to address space weather effects upon ionospherically dependent systems, Radio Sci., 44, RS0A29, doi:10.1029/2008RS004083, [printed 45(1), 2010]

RADIO SCIENCE, VOL. 44, RS0A29, doi:10.1029/2008RS004083, 2009

A Frequency-Agile Distributed Sensor System to address space weather effects upon ionospherically dependent systems

D. D. Rice,[1] J. V. Eccles,[1] J. J. Sojka,[1] J. W. Raitt,[1] J. Brady,[1] and R. D. Hunsucker[2]

Received 31 October 2008; revised 18 May 2009; accepted 8 July 2009; published 22 September 2009.

[1] The outstanding problem faced by operational systems that utilize the ionosphere is that ionospheric weather variability is comparable to the ionospheric climate variability. However, the number of simultaneous measurements is orders of magnitude too few to resolve the weather scales that are impacting systems. We describe a prototype distributed array of affordable passive radio beacon monitors combined with a central data repository and a data-model analysis system called the Frequency-Agile Distributed Sensor System (FADSS). By monitoring signals from terrestrial VLF/HF radio beacons the FADSS tracks changes in the *D*, *E*, or *F* regions and makes appropriate modifications to the ionospheric specification in near real time. These observations provide fundamental seasonal and diurnal climatology and weather affecting the lower ionosphere. They demonstrate space weather effects on communications over the VLF through HF range, even during quiet solar minimum conditions.

Citation: Rice, D. D., J. V. Eccles, J. J. Sojka, J. W. Raitt, J. Brady, and R. D. Hunsucker (2009), A Frequency-Agile Distributed Sensor System to address space weather effects upon ionospherically dependent systems, *Radio Sci.*, *44*, RS0A29, doi:10.1029/2008RS004083.

1. Introduction

[2] Knowledge of the terrestrial ionosphere is important to scientific research and to operational users in both the private and public sectors. While researchers have made much progress in understanding the mechanisms and climatology of the ionosphere in the last century, the impacts and phenomena associated with space weather remain an active research area; the morphology and evolution of many space weather events are poorly understood. Weather events can have severe effects on operational users, including sudden ionospheric disturbances (SIDs) experienced by Navy communicators and navigation aids at very low frequencies (VLF); link degradation and blackouts experienced by high-frequency (HF) long-distance communicators; and refraction, long phase delays, and scintillations experienced on trans-ionospheric very high and ultrahigh frequency (VHF, UHF) satellite channels that increase bit error rates and produce position errors and loss of lock for satellite-based navigation systems.

[3] Active radio-based methods of studying the ionosphere have provided much of the information about ionospheric physics since the early twentieth century [see, e.g., *Hunsucker*, 1991, chapters 3–5 and 9]. However, active methods such as vertical and oblique ionosondes, incoherent scatter radars, and spaced receiver interferometry require expensive transmitters, time-consuming government spectrum allocations and authorizations, and large antenna arrays. Potential problems with interference to other spectrum users often prevent active instruments from being located close to other research or communications facilities.

[4] A less-intrusive and potentially less expensive means of studying the ionosphere is to infer ionospheric conditions from the propagation of signals from existing transmitters at various frequencies. Transmitters with known, reliable characteristics are referred to as beacons. Many transmitters serve as dedicated beacons for real-time channel evaluation (RTCE), while others (such as standard time stations and navigation aids) are suitable for use as "beacons of convenience."

[5] Various ionospheric studies based on HF beacon propagation have been performed over the years [e.g., *Silberstein*, 1952; *Bixby*, 1956; *Porter*, 1966; *Shepherd and Lomax*, 1967]. The studies were typically performed for short periods (a few days or weeks) with one or two beacon transmitters. The decline of passive beacon studies is partly due to the problems encountered in these efforts. One problem is positively identifying the transmission source: in order to have a meaningful

[1]Space Environment Corporation, Providence, Utah, USA.
[2]RP Consultants, Klamath Falls, Oregon, USA.

0048-6604/09/2008RS004083$11.00

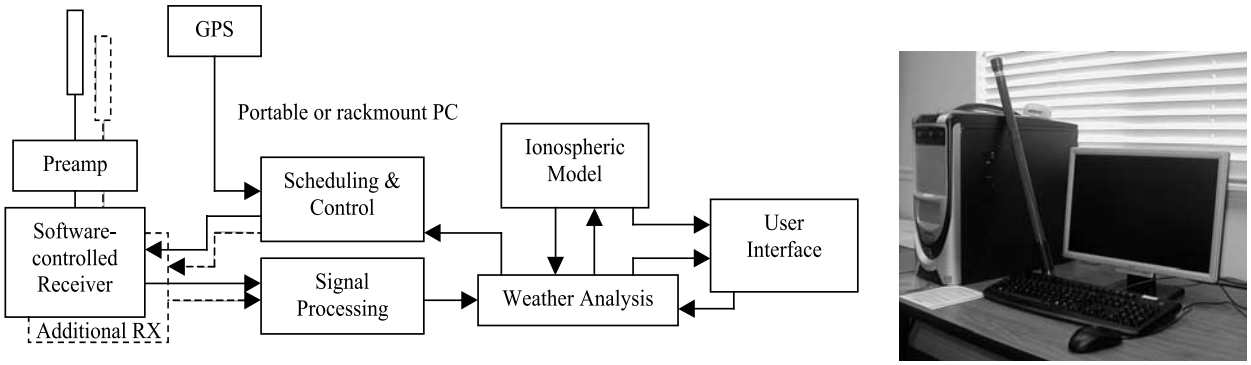

Figure 1. Conceptual sensor design including software block diagram and photo. The sensor consists of a Linux PC, a GPS receiver on top of the PC case, and a wideband active antenna leaning against the PC. The antennae are installed outdoors at roof level when deployed.

analysis, the received signal strength must be due to the desired beacon and not to other transmitters on or near the frequency of interest. A second problem is the complexity of modeling the ionospheric signal path and estimating the signal strength. A third problem is finding suitable beacons at appropriate ranges (typically 500–2000 km.) More recent HF beacon studies such as PENEX [*Hunsucker*, 1999] and various experiments related to HF backscatter radar have relied on dedicated beacons designed for those studies, and are therefore not strictly examples of passive monitoring. Recent interest in beacon monitoring has focused on VLF signals, which provide *D* region information, and satellites, specifically GPS measurements, which provide *F* region information such as total electron content (TEC) and scintillation data.

[6] A more fundamental problem with current research efforts is that ionospheric observations are sparsely distributed over large geographical areas due to the size and expense of active instruments. *Sojka et al.* [2004] argued that this approach cannot answer long-standing questions in space weather and upper atmospheric dynamics. A different observing strategy is needed, similar to that employed during the International Geophysical Year, which saw numerous studies conducted along chains of sites, allowing the spatial and temporal morphology and evolution of various phenomena to be recorded and analyzed. The key to such studies is the availability of small, low-cost instruments that can be widely deployed. Such an approach has been called for in the National Research Council's Decadal Research Strategy [*National Research Council*, 2003] and is being pursued through the Distributed Array of Small Instruments (DASI) initiative.

[7] With the advent of software radio technology, quantitative and affordable monitoring and analysis of radio beacons across a broad spectrum becomes possible. In this paper, we describe a prototype distributed array of affordable passive radio beacon monitors combined with a central data repository and data-model analysis. The network of beacon monitors is called the Frequency-Agile Distributed Sensor System (FADSS). The FADSS tracks regional changes in the *D*, *E*, or *F* regions and makes appropriate modifications to the ionospheric specification and user products in near real time with a 15-min cadence. Section 2 presents an overview of the frequency-agile sensors and the integrated distributed sensor system FADSS. Section 3 describes some FADSS data products obtained from VLF and HF propagation analysis. Section 4 presents a more detailed analysis of an M-class X-ray flare event affecting both VLF and HF communications.

2. FADSS System

2.1. SWARE Design

[8] The individual sensors comprising the FADSS are called Space Weather Aware Receiver Elements (SWAREs.) Each SWARE is a software-controlled, passive radio beacon monitor with capabilities for monitoring the signal strength of widely distributed transmitters from VLF through HF. Each sensor also integrates a GPS receiver for position and timing information; variations in the reported position of a SWARE in a fixed location may be an indicator of ionospheric weather influences on L-band propagation. The SWARE design is based on a WinRadio G313i PCI receiver card covering 9 kHz to 30 MHz, an LF Engineering L900/BNC compact active antenna, a Garmin GPS-17 receiver, and a standard Linux PC (Figure 1).

[9] The critical component of the SWARE is the suite of specialized software that controls the receiver, analyzes the received beacon signals, and provides meaningful assessment of the ionosphere and signal propagation

characteristics based on the observations. The unit is said to be "space weather aware" because it uses geophysical data sets, the signal observations, and modeling to arrive at an assessment of space weather conditions. Development efforts are aimed at enhancing the 'cognitive' abilities of the SWARE, using these data together with knowledge of the receiver's position and time to dynamically schedule observations of beacons through expert system logic, with attention on transmitter paths and beacon frequencies that provide the most information for current space weather conditions. When linked in real time with other SWAREs through the central data repository, the FADSS system is created. The collaborative power of this Distributed Array of Small Instruments (DASI) increases the space weather awareness of each SWARE, allowing the units to determine the geographical extent of observed anomalies and to exclude local perturbations at individual sites.

[10] Data collection and exchanges between the SWAREs and the CDR operate at a 15-min cadence. The SWARE collects data from various beacons and the GPS receiver for 15 min, while concurrently running ionospheric model and propagation analysis software. At the end of the period, collected data and model results are sent to the CDR. The SWARE also collects geophysical data, software updates, and other information from the CDR every 15 min.

[11] Each SWARE maintains its own model of the ionosphere to create a regional near-real-time electron density specification used to analyze the radio propagation paths from the beacons to the monitor. The International Reference Ionosphere [*Bilitza*, 2001] or the Ionospheric Forecast Model [*Schunk et al.*, 1997] is used for the *F* region and is combined with the DDDR (Data Driven *D* Region) [*Eccles et al.*, 2005] model for the *E* and *D* regions. The DDDR model is a simple ion chemistry model of the *D* region designed to incorporate sufficient positive and negative ion chemistry to generate an appropriate electron density for a wide range of natural geophysical conditions. These physics-based models make use of current geophysical indices and GOES X-ray observations obtained from the CDR.

[12] HF propagation analysis is carried out with C. Coleman's HASEL ray-tracing program [*Coleman*, 1993] using the model electron density specification. VLF waveguide propagation analysis is performed using the Long Wave Propagation Capability (LWPC) [*Ferguson*, 1998]. Comparison of observed propagation with these model predictions allows space weather conditions to be inferred.

[13] The standard SWARE has been developed for operation in a normal office environment, where power and Internet communications are readily available. A special transportable unit has also been developed that can operate from 12 VDC power, e.g., battery or solar panels, in a field environment. Each SWARE currently costs between $5K and $15K depending on options.

2.2. Frequency Selection

[14] The SWARE receiver and active antenna cover 9 kHz through 30 MHz. Expanded coverage through 140 MHz is available with a receiver add-on and an additional antenna, but the 30 MHz upper limit is suitable for most midlatitude applications.

[15] Figure 2 shows a summer ionospheric density profile expressed in terms of critical frequency. Figure 2 gives a rough idea of the ionospheric region that various radio frequency signals interact with: VLF (3–30 kHz) and LF (30–300 kHz) are affected by the *D* region bottomside; MF (300–3000 kHz) interacts with night *E* region ionization, some late nighttime *F* regions, and most of the daytime *E* region bottomside; and the HF range (3–30 MHz) is affected by normal midlatitude *E* and *F* region profiles and sporadic *E*.

[16] In order to infer information about the ionosphere, the FADSS requires reliable, identifiable signals propagating over moderate distances (about 500–2000 km.) Many sources of such signals exist in the various bands.

[17] In the VLF band, powerful transmitters used for navigation and naval communications are available worldwide. In North America, transmitters of interest include naval stations NAA, NLK, NML, and NPM in the 20–26 kHz range.

[18] At LF, numerous low-to-moderate power transmitters are available, including standard time stations (WWVB), navigation (LORAN), and aeronautical nondirectional beacons.

[19] MF is less promising for beacon monitoring, because the bulk of the frequency range is used for AM broadcasting in North America and many other parts of the world. AM broadcasters cannot be easily identified by signal analysis, and most frequencies are shared by several stations in different regions. Thus beacon monitoring is limited to navigational aids at lower MF (300–500 kHz), and a few reliable transmitters (such as WWV) at the high end, 1.8–3 MHz.

[20] HF offers a variety of potential beacons, including standard time stations such as WWV/WWVH, and various amateur radio beacons.

[21] In this paper, we focus on VLF transmitters NLK and NML, and HF standard time station WWV to illustrate the collection of space weather data by the SWAREs. These transmitters are summarized in Table 2.

2.3. FADSS Description

[22] While each SWARE acts as a stand-alone propagation monitor, it is most useful when cooperating with other monitors connected to the Frequency-Agile Distributed Sensor System. The cooperative sharing of data and analysis allows for substantial increase in fidelity of

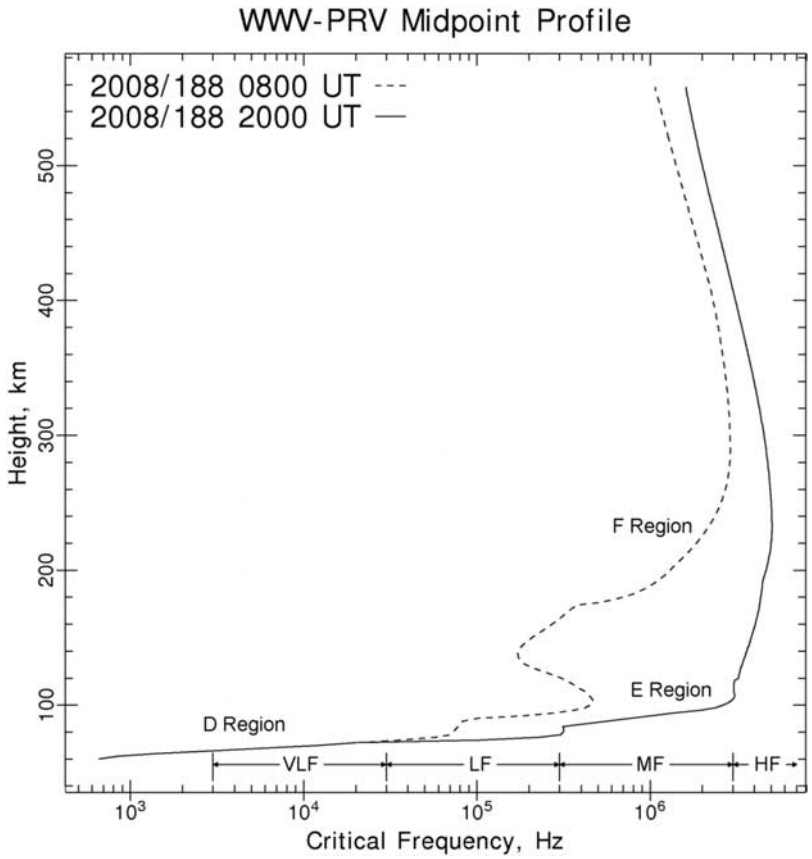

Figure 2. Model summer ionospheric density expressed as critical frequency. The solid line corresponds to local noon, and the dashed line corresponds to local midnight.

the space weather assessment provided by FADSS. The networked system is composed of SWAREs connected by the Internet to a Central Data Repository (CDR). The CDR receives observations and analysis conclusions from each SWARE in the network, and then combines these results into a unified specification of the regional space weather conditions. The number of observations to blend into the ionosphere specification grows with the spatial density and spectral density associated with increasing numbers of SWAREs. The growth in computational needs of the network is met by utilizing the computational power associated with each SWARE. Most of the data analysis and data-model inversion takes place on each SWARE computer. The CDR then combines the individual SWARE results into a unified product, which can then be accessed by the FADSS users.

[23] In addition to serving as the central computational modeling facility where the regional ionospheric weather structures can be reconstructed, the CDR allows SWARE operations to be optimized by informing the SWAREs of overall propagation conditions. For example, if sporadic *E* is detected by a few SWAREs, this information will allow the other SWAREs to examine adjacent frequencies and paths to try to determine the extent of the sporadic *E* effects. Another example would be communications blackouts caused by solar flare absorption; initial estimates of absorption by the CDR would allow SWARE resources to be shifted away from blacked out frequencies to monitor the flare recovery and other ionospheric effects.

2.4. FADSS Initial Deployment

[24] The base FADSS network in the western United States for our initial deployment relies on three SWAREs: Bear Lake Observatory (BLO) in northern Utah, maintained by Space Environment Corporation; Klamath Falls (KFO), Oregon, maintained by R. Hunsucker; and Tucson (TUC), Arizona, maintained by J. Raitt. These three locations form a triangle with an 860 km east-west alignment between BLO-KFO and a 1,085 km north-south alignment between BLO-TUC (Figure 3). The baselines then provide the outer spatial scale, 1000 km, for the

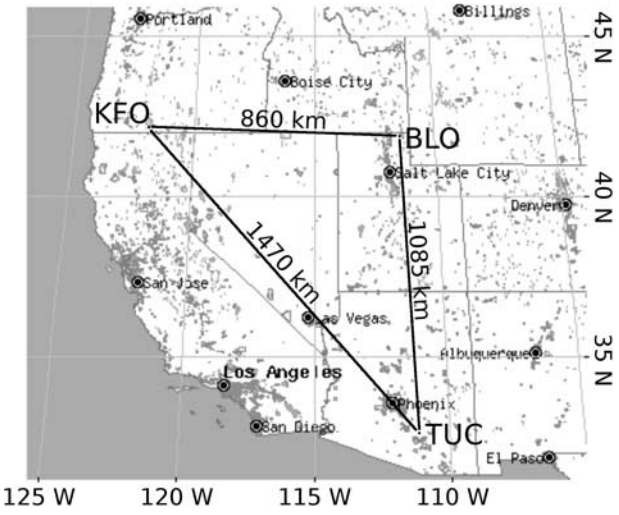

Figure 3. Base observational network completed in November 2007 in the western United States. Shaded areas are populated regions.

FADSS to study ionospheric structures. These three FADSS sites became operational between September and November 2007.

[25] In addition to the three primary SWARE deployments at BLO, KFO, and TUC, a fourth SWARE has been deployed in Baker City, Oregon (BKR) since July 2008. Three other SWAREs are deployed near Providence, Utah for development and testing purposes. These are in River Heights (PRV), at the Space Environment Corporation offices (SEC), and in Logan (LGN), Utah. The separation between these three is less than 10 km and the group lies about 40 km southwest of BLO. Table 1 lists the location of the SWAREs. Operationally, they follow the same monitoring schedule as the primary deployment triangle and all operate in real time. Space Environment Corporation provides public access to FADSS observations at http://www.spacenv.com/∼agile. Table 2 lists the monitored transmitters, their frequencies, and their locations and provides the distance to the three base FADSS nodes shown in Figure 3.

3. FADSS Observational Products

[26] Numerous data products may be extracted from the analysis of FADSS signal propagation results and comparisons with the ionospheric model. In this section, three observation products are briefly described; climatology of RF propagation characteristics, two-dimensional maps of sporadic *E*, and anomalous HF absorption associated with NO transport during winter months.

3.1. Long-Term Observations

[27] The observational database collected by FADSS extends the WWV signal strength data collection that began in late 2002 [*Eccles et al.*, 2005] and included major geomagnetic storms and record X-ray flare events. In addition to this HF data, VLF signal data are being added, documenting the prolonged solar minimum conditions of the last 2 years. Initial VLF data were recorded using receivers designed for the Stanford IHY SID project, prior to the deployment of the SWAREs. The complete 2007 VLF data set of the NML to PRV path obtained from the Stanford IHY SID receiver is shown in Figure 4.

[28] The signal strength is shown as a function of UT and day of year with lighter tones representing strong signal strength. The very distinctive hourglass shape is due to the seasonal variation of daylight hours. The area inside the hourglass shape is nighttime, where maximum signal levels are usually observed. The narrowest section of the hourglass is summer solstice. The bottom of the hourglass is January, and the top is December. The series of regularly spaced black horizontal stripes between 1200 and approximately 2000 UT represent once-per-week maintenance outages of the NML transmitter. White areas are missing data caused by failures at the receiver site. It is important to note that the diurnal variations of VLF signals depend on the earth-ionosphere waveguide between the transmitter and receiver; different paths can have quite different diurnal signal variations.

[29] For the NML-PRV path there is a well defined signal strength minimum at dawn and dusk. These low signal strength periods at dawn and dusk are due to the rapidly changing *D* region effective height. As the receiver and/or the transmitter crosses the solar terminator the *D* region suffers a rapid change density contour heights which disrupts a simple earth-ionosphere waveguide for VLF propagation. This produces destructive interference between the ground wave and propagating sky wave modes to produce the lowest signal strengths of the UT day. The dawn crossing signature (right side of the hourglass) is narrower than the dusk crossing (left

Table 1. FADSS Beacon Monitor Locations

Receiver ID	Location	North Latitude	East Longitude	Altitude (m)
BLO	Bear Lake Observatory, UT	41.934	−111.421	1973
BKR	Baker City, OR	44.789	−117.833	1048
KFO	Klamath Falls, OR	42.173	−121.850	1320
LGN	Logan, UT	41.731	−111.807	1460
PRV	River Heights, UT	41.720	−111.822	1395
SEC	Providence, UT	41.712	−111.830	1383
TUC	Tucson, AZ	32.437	−110.982	875

Table 2. VLF and HF Beacons in the Western United States

Transmitter	Latitude (deg N)	Longitude (deg E)	Frequency (kHz)	BLO Distance (km)	KFO Distance (km)	TUC Distance (km)
NAA	44.636	−67.230	24.0	3,540	4,355	3,980
NPM	21.446	−158.133	21.4	4,900	4,085	4,795
NLK	48.202	−121.931	24.8	1,080	670	1,980
NML	46.362	−98.295	25.2	1,155	1,920	1,885
WWV	40.681	−105.041	2,500, 5,000, 10,000, 15,000, 20,000	580	1,410	1,080
WWVH	21.988	−159.764	2,500, 5,000, 10,000, 15,000	4,950	4,170	4,930

side), and the dawn signature is narrowest in summer. The narrow dawn signature of the summer is consistent with the solar zenith angle changing more rapidly during summer dawn than during winter dawn. The wider terminator signature of the dusk crossing is due to the time-dependent decay of the *D* region bottomside at the very low electron densities (∼10/cc), which defines the ionospheric boundary of the waveguide for VLF propagation. The dusk boundary is indistinct at times during the winter, suggesting that small gradients at winter dusk reduce the degree of destructive interference.

[30] The nighttime VLF signal levels are higher than daytime levels (Figure 5, top) and also have much greater variability in time (Figure 5, bottom). The nighttime *D* region effective height is sensitive to gravity waves causing greater VLF signal strength variability. The daytime *D* region effective height is set by the steady solar ionization, which limits the signal strength variability.

[31] Some seasonal effects in Figures 4 and 5 have less obvious causes. Daytime signal levels increase abruptly in mid-April and decrease again in October. A gradual shift between winter and summer signal levels is expected due to higher summer sun angles, but the abrupt change suggests that another cause, such as a seasonal change in mesospheric wind patterns. The nighttime signal levels also drop during the fall. The day-to-day variability in the daytime signal levels decrease substantially during the elevated signal of the summer (May through September). Day-to-day daytime variability for summer and winter might be explained by the *D* region sensitivity to NO densities. During the summer time wind pattern of the mesosphere and the higher solar angle increases the loss of NO and imposes an equilibrium profile and reduces the daytime variability. During the winter the NO densities can change substantially due to the longer periods of darkness. The day-to-day changes in the daytime signal strength during the winter season are presumed to be cause by variations in mesospheric neutral winds variations. Winter time changes in the NO profile has similar influences on HF absorption variability 0020 [*Kawahira*, 1985].

3.2. Sporadic *E*

[32] Midlatitude sporadic *E* is thought to be caused by wind shears, and the winds are affected by tides and atmospheric waves [*Whitehead*, 1989; *Mathews*, 1998]. At present, the most practical way to include sporadic *E* in ionospheric specifications is to ingest observations. Sporadic *E* may be inferred from HF signal observations when significant signal levels are recorded at frequencies well above the maximum usable frequency indicated by the model analysis.

[33] During July 2008, SWAREs were deployed to various locations in Nevada, Oregon, and Idaho in order to detect and map summer sporadic *E*. Figure 6 shows one sporadic *E* map for 7 July 2008 (day 189) at 0000 UT, with squares indicating the minimum sporadic *E* critical frequency required to provide 20 MHz WWV propagation on the indicated path. In addition to SWARE data, FADSS ingested data from 28 and 50 MHz beacon observations by the amateur radio PropNet project [*Ford*, 2008], and the CADI ionosonde at BLO (diamond.) The CADI indicated sporadic *E* critical frequencies exceeded 9 MHz during this observation.

[34] The model analysis is shown in Figure 7. Figure 7 (left) shows the 20 MHz WWV rays for the model ionosphere without sporadic *E,* and Figure 7 (right) shows propagation with the addition of a 9 MHz sporadic *E* layer based on CADI observations. The model shows this sporadic *E* layer providing propagation to distances greater than 450 km from WWV. Together with Figure 6, these observations provide evidence of sporadic *E* blanketing much of the western United States at that time.

[35] The goal for mapping sporadic *E* is to have HF path midpoints separated by about 150 km or less.

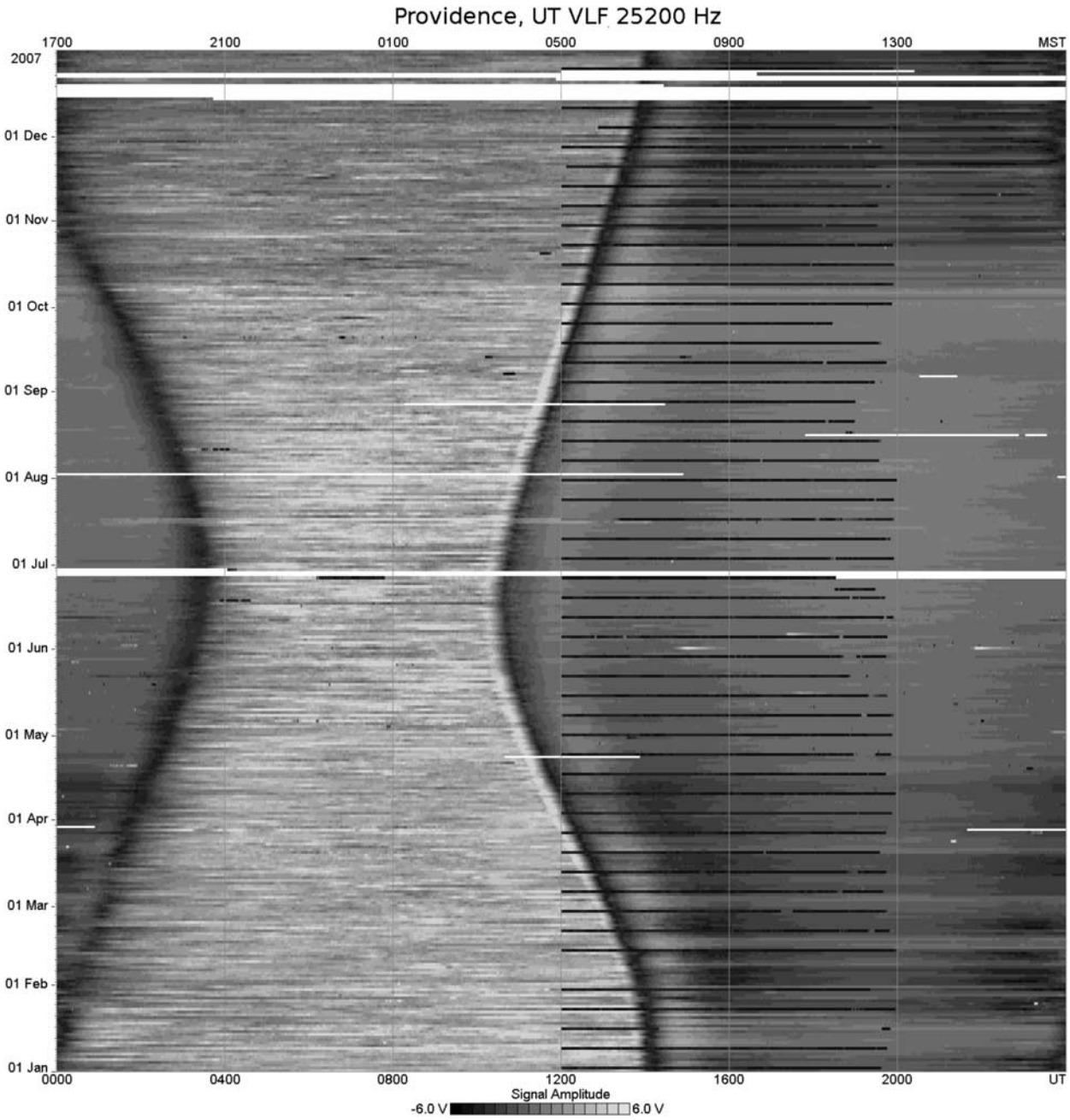

Figure 4. Signal strength observations for 2007 from the Stanford NML receiver in Providence, Utah.

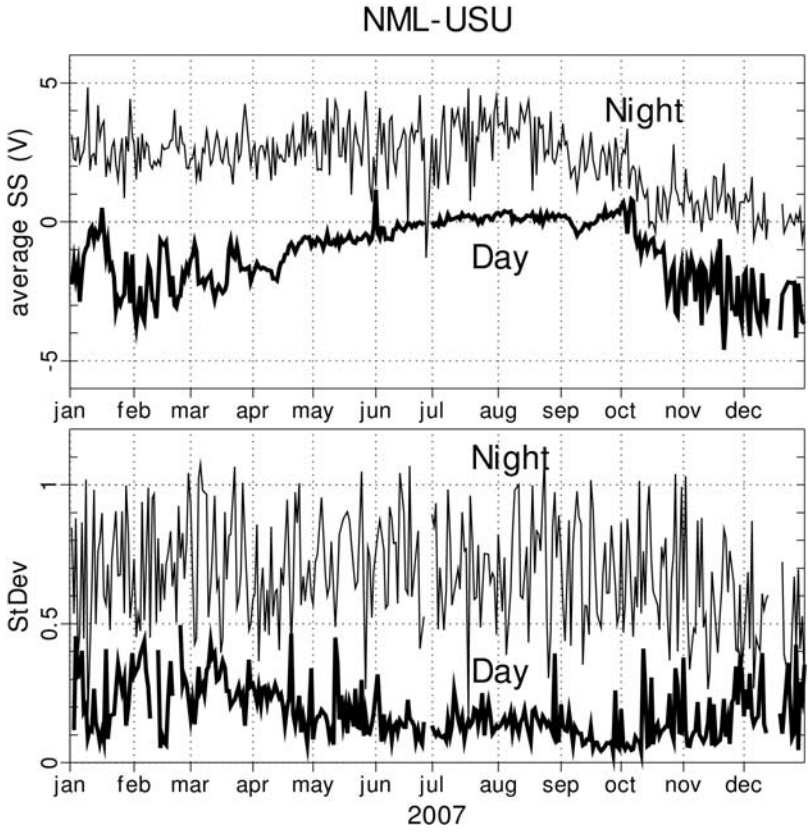

Figure 5. (top) Plot average signal strength for nighttime (0500–0900 UT) and daytime (2000–2200 UT). (bottom) Standard deviation of signal strength with time for daytime and nighttime signal during the same UT ranges. Daytime values are plotted with thick line.

Achieving this goal will require deploying more SWAREs and monitoring additional HF transmitters. The current FADSS allows maps similar to Figure 5 to be generated at regular intervals.

3.3. *D* Region Weather

[36] The *D* region is responsible for nondeviative absorption, which attenuates signals propagating through the *D* region. Normal daytime absorption can cause noticeable signal attenuation at frequencies up to 10–15 MHz, and often completely eliminates sky wave signals below 5 MHz.

[37] At VLF through lower LF, the *D* region bottomside provides the upper surface of the earth-ionosphere waveguide, and these signals are reflected rather than absorbed. The *D* region continues to reflect VLF signals at night, due to continued ionization from cosmic rays and geocorona. Thus VLF propagation provides a diagnostic of the very tenuous nighttime *D* region.

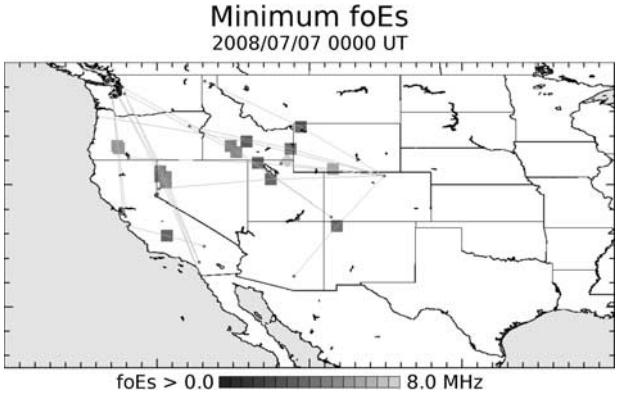

Figure 6. Map of sporadic *E* propagation over 1 h in the western United States, based on data from SWAREs, PropNet, and the BLO CADI.

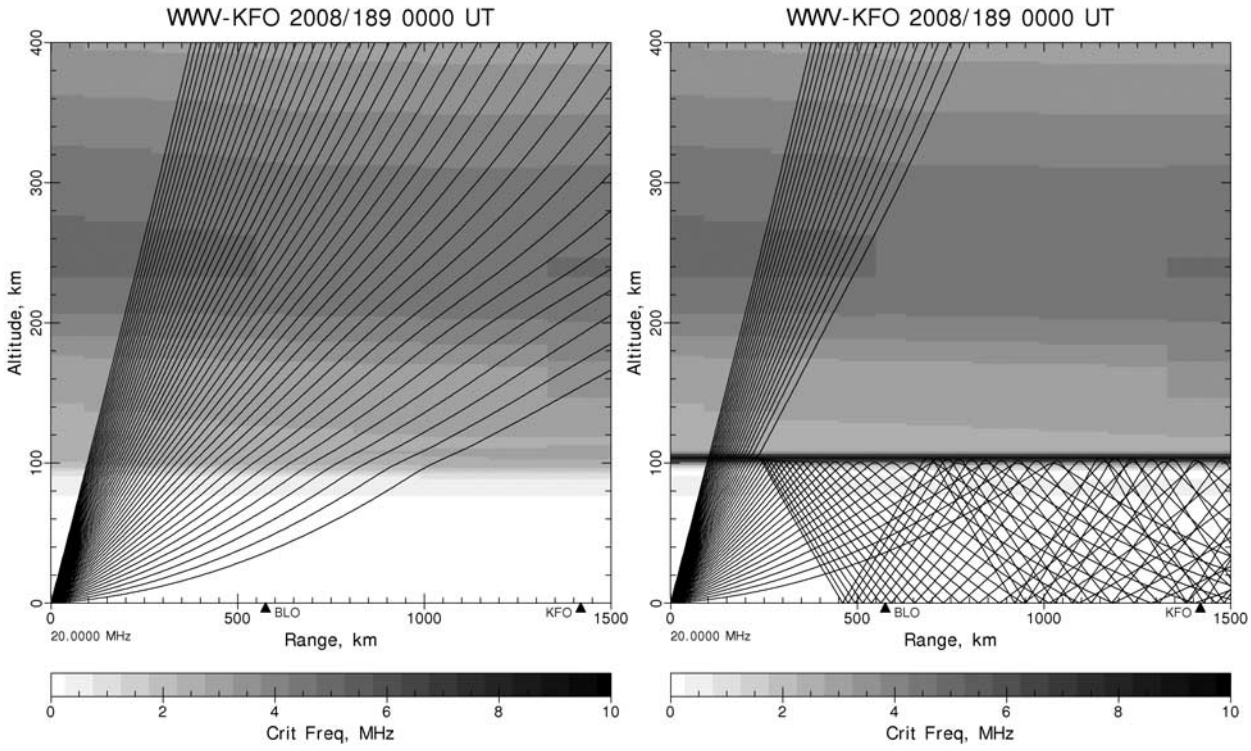

Figure 7. Modeled 20 MHz propagation (left) without sporadic *E* and (right) with a 9 MHz sporadic *E* layer.

[38] Figure 8 illustrates the winter absorption anomaly, long observed at HF [*Schwentek*, 1974], in which daytime absorption levels vary by tens of decibels over the period of several days. It is believed to be related to the transport of nitric oxide (NO) from polar regions by winds influenced by planetary waves [*Kawahira*, 1985].

[39] The NLK-KFO path is over Washington and Oregon, while the WWV-PRV path crosses southwestern Wyoming. Thus the enhanced VLF signal in Figure 8 may indicate NO flowing from higher latitudes and eventually reaching the lower-latitude WWV-PRV path, where it results in higher daytime absorption. Monitoring the VLF transmitters near the Canadian border (NLK, NML, NAA) may therefore provide warning of midlatitude HF absorption episodes.

4. X-Ray Flare Effects

[40] The FADSS deployment has occurred during the ongoing lengthy solar minimum period, so there have been few significant space weather events thus far. One took place on 25 March 2008, when an M-class X-ray flare produced effects in HF and VLF signals at most SWAREs. The responses are described below.

4.1. HF Absorption

[41] X-ray flare effects on the WWV signal path were studied in the prior HIDIVE study and described by *Eccles et al.* [2005]. The flare causes increased ionization of the *D* region [*Thomson et al.*, 2005], so HF paths traversing the dayside *D* region experience sharp increases in absorption. The flare response for the 25 March flare is shown in Figure 9.

[42] The X-ray flare peaked at 1900 UT, then gradually returned to lower levels over the next few hours. This timing is reflected in the HF signal absorption, with signal levels dropping by more than 10 dB at 1900 UT. The 5 MHz PRV signal shows the greatest absorption; the 10 MHz KFO and TUC signals show somewhat less absorption. In general absorption is inversely proportional to the square of the signal frequency.

[43] Automatic identification of flare signatures in HF data is difficult due to the large variations normally seen in HF signal levels. In Figure 9, it would be difficult to distinguish the flare response in the 10 MHz

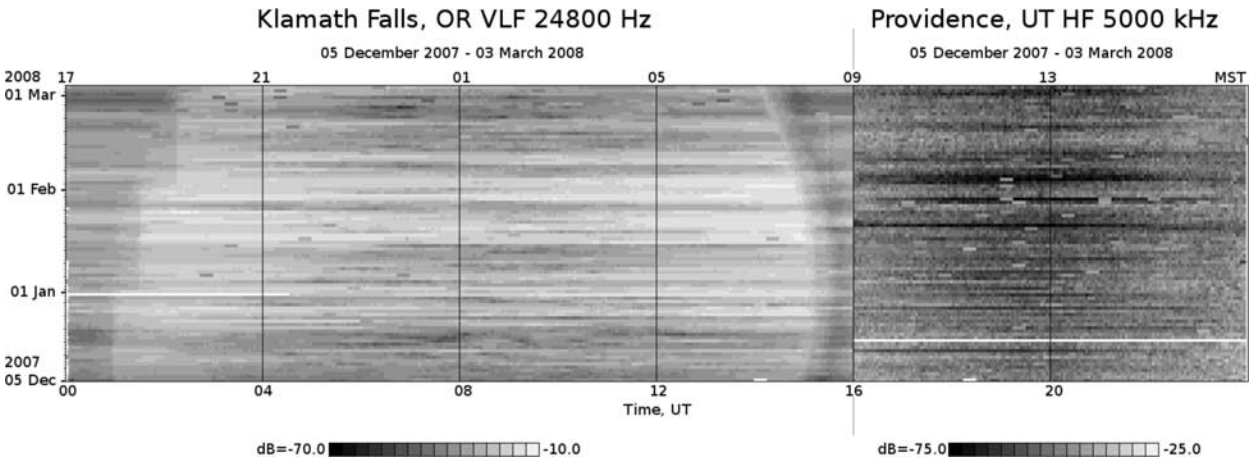

Figure 8. (left) Nighttime VLF propagation from NLK to KFO (0000–1600 UT) and (right) daytime HF propagation from WWV to PRV (1600–2400 UT) showing the relationship between VLF signal enhancement and HF absorption during the winter (5 December 2007 through 3 March 2008).

data from other effects. Flare signatures are not seen in the lower-frequency signals (PRV 2.5 MHz; KFO and TUC 2.5 and 5 MHz) because those signals were already absorbed by the normal daytime *D* region. These limitations motivated the expansion of FADSS frequency range to cover VLF and LF in addition to HF used in the previous HIDIVE study.

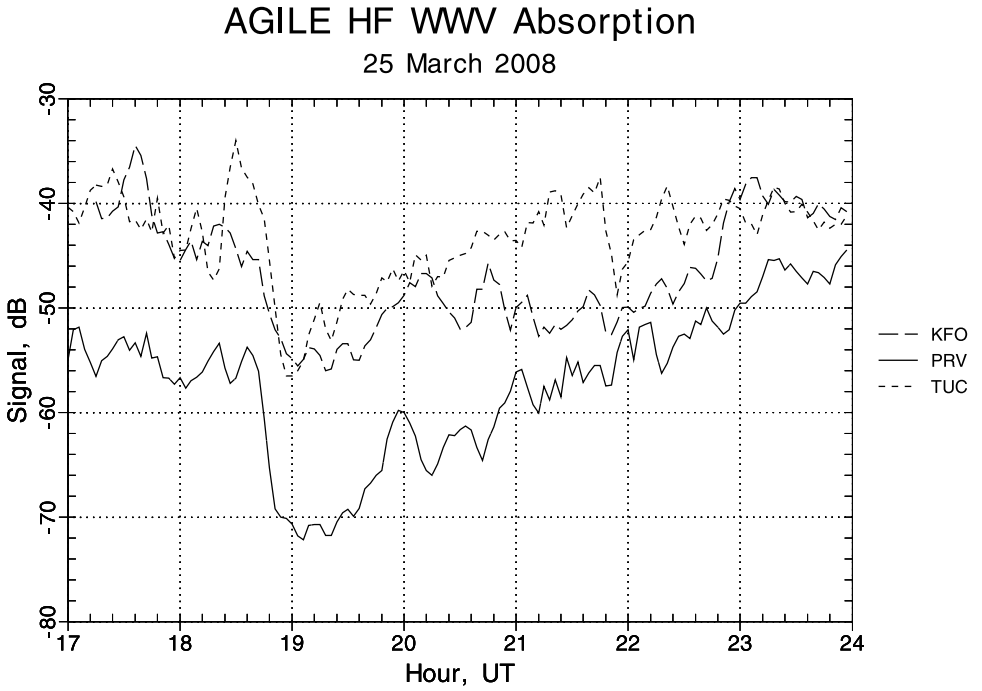

Figure 9. HF response to an M-class X-ray flare. The flare peak occurred at 1900 UT. PRV is the 5 MHz WWV signal; KFO and TUC are 10 MHz WWV signals.

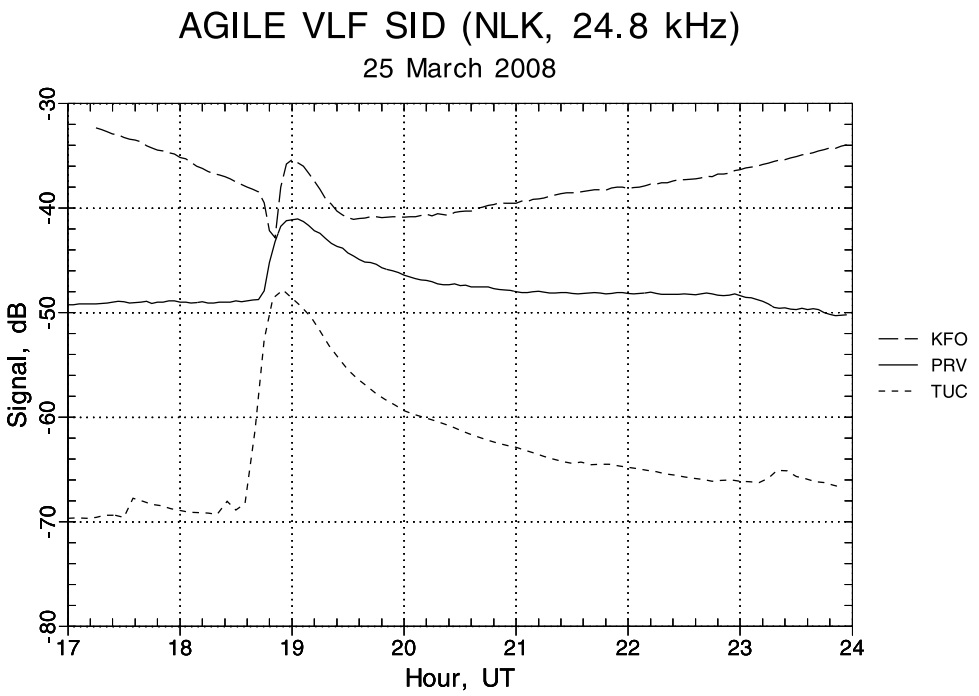

Figure 10. VLF response to the M-class X-ray flare (bottom trace).

4.2. VLF Sudden Ionospheric Disturbance

[44] At VLF, the X-ray flare enhancement of the *D* region causes a sudden constriction of the earth-ionosphere waveguide over the entire daylight hemisphere. For moderate VLF paths, this constriction often causes an increase in signal strength, but for some geometries the signal level may drop. The VLF flare response for 25 March is shown in Figure 10.

[45] The flare peak at 1900 UT produces a simple increase in signal on the NLK-PRV path, giving a "typical" SID signature. However, an initial sharp decrease in signal on the NLK-KFO path occurs before the increase. As the effective reflection height of the *D* region drops rapidly during the X-ray flux increase, it produces destructive interference briefly on the NLK-KFO path. Such distinctive behaviors can assist in the modeling and inversion process.

[46] The important feature of the VLF SID response is that, unlike HF, it has a well-defined signature relative to the normal relatively constant daytime signal behavior. When two or more VLF signals are available, the SWARE has a reasonable chance of reliably identifying SIDs and applying the information to the HF analysis as well. Note that, due to the 15 min update cadence, an X-ray flare may be well underway before the SWARE receives GOES data confirming the event, so the ability to recognize the SID quickly is important.

4.3. Modeling

[47] The ionospheric model of the X-ray flare response is shown in Figure 11. The *D* region electron density profile is determined by calculating the ionization profile during the flare X-ray flux then solving the *D* region ion chemistry response at each altitude. The *D* region bottomside drops several kilometers in response to the flare and in fact drops below the model's 60 km starting altitude. These profiles are used in the propagation analyses. The 5 MHz WWV-PRV model signal is shown in Figure 12.

[48] The HF propagation model shows good agreement with the average HF signal prior to the flare and through its onset, peak, and recovery. The *D* region model generally provides a good description of moderate X-ray flares; this capability is missing from most currently available propagation modeling tools.

5. Conclusions

[49] A low-cost, miniature, frequency-agile beacon monitor has been developed as the building block for a Frequency-Agile Distributed-Sensor System (FADSS) that can map important quantities such as sporadic *E* and *D* region absorption in the lower ionosphere and upper atmosphere. The stand-alone beacon monitor is a

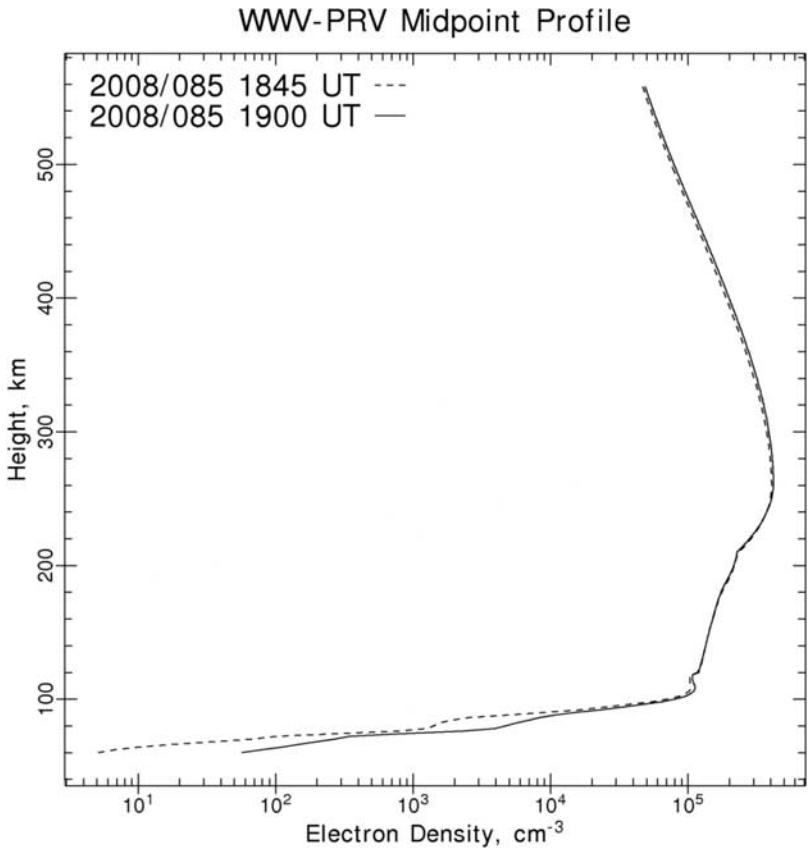

Figure 11. Ionospheric model of X-ray flare response. The electron density profile prior to the flare (dashed line) shows higher *D* region bottomside compared to the profile at the flare peak (solid line).

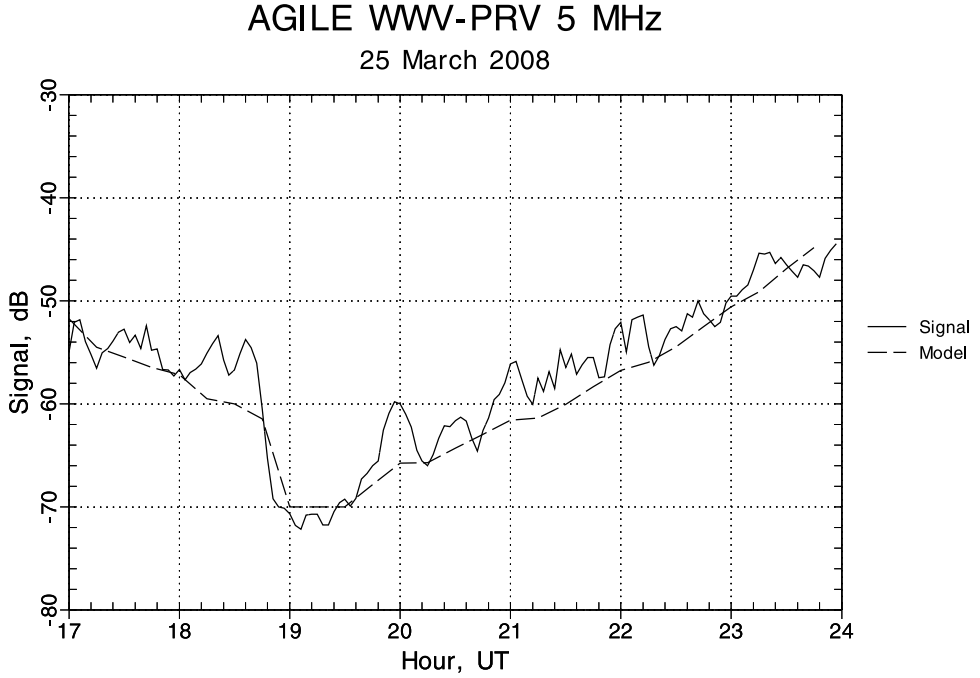

Figure 12. Model signal propagation (dashed) and observed signal strength (solid).

sophisticated measurement tool designed to collect observations of several transmitters over a wide frequency range, with accurate time and position information provided by its GPS receiver. The beacon monitor also runs ionospheric and signal propagation models to establish a local space weather specification. However, it is the cooperative sharing of data and model results in a distributed network of monitors that provides the ability to map space weather not previously possible.

[50] The initial FADSS deployment has provided several proof-of-concept results that will enable the project to make real-time ionospheric weather and structure mapping possible. It has collected data showing winter absorption anomaly and X-ray flare effects on the *D* region at both VLF and HF. Maps of summer sporadic *E* have been generated using temporary field deployments of SWAREs, and the integration of data from the BLO CADI ionosonde and other beacon monitoring efforts has been demonstrated. Moving these capabilities from the experimental stage into production operation is currently underway.

[51] The primary objective for future development is to increase coverage by adding more SWAREs to the FADSS and by increasing the number of beacons being monitored. Deployment at higher latitudes is planned to test the modeling and analysis software in the more complex and dynamic subauroral environment.

[52] **Acknowledgments.** This research was supported by SBIR II contract FA8718-07-C-0016 from AFRL at Hanscom AFB to Space Environment Corporation. The VLF SID Space Weather Monitor is an instrument developed through a project sponsored by Stanford University, the National Science Foundation, NASA, and is part of the United Nations' International Heliospherical Year, 2007. See http://sid.stanford.edu for project information and data. We also wish to acknowledge the contribution of many radio amateurs through the PropNet project (http://www.propnet.org).

References

Bilitza, D. (2001), International Reference Ionosphere 2000, *Radio Sci.*, *36*, 261–275, doi:10.1029/2000RS002432.

Bixby, L. H. (1956), Interpretation of WWV and WWVH signal strength variations at Stanford, Ph.D. dissertation, Stanford Univ., Stanford, Calif.

Coleman, C. J. (1993), A general purpose ionospheric ray tracing procedure, *Rep. SRL0131TR*, Def. Sci. and Technol. Org., Edinburgh, South Aust., Australia.

Eccles, J. V., R. D. Hunsucker, D. Rice, and J. J. Sojka (2005), Space weather effects on midlatitude HF propagation paths: Observations and a data-driven *D* region model, *Space Weather*, *3*, S01002, doi:10.1029/2004SW000094.

Ferguson, K. (1998), Computer programs for assessment of long-wavelength radio communications, version 2.0, *Tech. Doc. 3030*, pp. 92,152–95,001, Space and Nav. Warfare Syst. Cent., San Diego, Calif., May .

Ford, S. (2008), PropNET, *QST*, *92*, 95.

Hunsucker, R. D. (1991), *Radio Techniques for Probing the Terrestrial Ionosphere*, *Phys. Chem. Space Ser.*, vol. 22, Springer, New York.

Hunsucker, R. D. (1999), Final report on PENEX data analysis project, Nav. Postgrad. Sch., Monterey, Calif.

Kawahira, K. (1985), The *D* region winter anomaly at high and middle latitudes induced by planetary waves, *Radio Sci.*, *20*, 795–802, doi:10.1029/RS020i004p00795.

Mathews, J. D. (1998), Review paper: Sporadic *E*: Current views and recent progress, *J. Atmos. Sol. Terr. Phys.*, *50*, 413–435, doi:10.1016/S1364-6826(97)00043-6.

National Research Council (2003), *The Sun to the Earth—And Beyond*, Natl. Acad. Press, Washington, D. C.

Porter, G. C. (1966), Measurement of polarization statistics of signals received over a short range HF path, *IEEE Trans. Commun. Technol.*, *14*, 484, doi:10.1109/TCOM.1966.1089347.

Schunk, R. W., J. J. Sojka, and J. V. Eccles (1997), Expanded capabilities for the ionospheric forecast model, *Rep. AFRL-VS-HA-TR-98–0001*, Air Force Res. Lab. Space Vehicles Dir., Hanscom AFB, Mass.

Schwentek, H. (1974), Some results obtained from the European cooperation concerning studies of the winter anomaly in ionospheric absorption, in *COSPAR Proceedings of the Methods of Measurements and Results of Lower Ionosphere Structures Symposium, Constance, Germany*, edited by K. Rawer, pp. 281–286, Comm. on Space Res., Paris.

Shepherd, R. A., and J. B. Lomax (1967), Frequency spread in ionospheric radio propagation, *IEEE Trans. Commun. Technol.*, *15*, 268, doi:10.1109/TCOM.1967.1089568.

Silberstein, R. (1952), Interpretation of high-frequency CW field intensity records with the aid of simultaneous pulse data, *Proc. IRE*, *40*, 974.

Sojka, J. J., D. Rice, J. V. Eccles, F. T. Berkey, P. Kintner, and W. Denig (2004), Understanding midlatitude space weather: Storm impacts observed at Bear Lake Observatory on 31 March 2001, *Space Weather*, *2*, S10006, doi:10.1029/2004SW000086.

Thomson, N. R., C. J. Rodger, and M. A. Clilverd (2005), Large solar flares and their ionospheric *D* region enhancements, *J. Geophys. Res.*, *110*, A06306, doi:10.1029/2005JA011008.

Whitehead, J. D. (1989), Recent work on midlatitude and equatorial sporadic *E*, *J. Atmos. Terr. Phys.*, *54*, 401–424, doi:10.1016/0021-9169(89)90122-0.

J. Brady, J. V. Eccles, J. W. Raitt, D. D. Rice, and J. J. Sojka, Space Environment Corporation, 221 North Spring Creek Parkway, Suite A, Providence, UT 84332, USA. (vince.eccles@spacenv.com)

R. D. Hunsucker, RP Consultants, 7917 Gearhart Street, Klamath Falls, OR 97601, USA.